

Synchronized molecular dynamics simulation via macroscopic heat and momentum transfer for polymer lubrication

Shugo Yasuda¹ * and Ryoichi Yamamoto² †

¹*Graduate School of Simulation Studies, University of Hyogo, Kobe 650-0047, Japan,*

²*Department of Chemical Engineering, Kyoto University, Kyoto 615-8510, Japan*

The synchronized molecular dynamics simulation is proposed to calculate the distribution of local stresses and temperatures in polymer lubrication. In this method, the molecular dynamics simulations which are assigned to small fluid elements to calculate the local stresses and temperatures are synchronized at a certain time interval to satisfy the macroscopic heat and momentum transport equations. This method is applied to the thermohydrodynamic lubrication of a polymeric liquid composed of short chains between parallel plates. The rheological properties and conformation of polymer chains coupled with the temperature rise caused by local viscous heating are investigated with a non-dimensional parameter, i.e., the Nahme-Griffith number, which is defined by the ratio of the viscous heating to the thermal conduction at the characteristic temperature required to sufficiently change the viscosity. The present simulation demonstrates that strong shear thinning and transitional behavior of the conformation of the polymer chains occurs with a rapid temperature rise when the Nahme-Griffith number exceeds unity. The results also clarify that the linear stress-optical relation holds despite the complicated behaviors of the temperature, the shear rate, and the conformation of the polymer chains.

PACS numbers: 47.11.St, 47.11.Mn, 47.85.mf, 83.10.Rs, 83.60.St

Keywords: multiscale modeling, polymer lubrication, viscous heating, rheology

In typical simulation studies, the nonlinear rheological properties of complex fluids are investigated through non-equilibrium molecular dynamics (NEMD) simulations with a thermostat; in these simulations, the velocity gradient and temperature are kept constant and uniform in the MD cell.^{1,2} However, in actual engineering systems, the rheological properties of the system are affected by the spatial heterogeneity caused by the momentum and energy transports involved in the boundary conditions. A typical example is the generation of heat in lubrication systems.³ To predict the behaviors of these complicated systems, the macroscopic thermohydrodynamics of the entire system must be considered on the basis of an appropriate molecular model. In principle, full MD simulations of the entire system can meet these requirements. However, it is practically difficult to perform full MD simulations on the macroscopic scale, which is common in actual engineering systems and is far beyond the molecular size. Multiscale modeling is a promising candidate to tackle this type of problem.^{4–24}

We have recently developed a multiscale simulation of MD and computational fluid dynamics (CFD) for the momentum transport of complex fluids. The multiscale method was first developed to the simple fluids¹⁵, and then extended to the polymeric liquids with the memory effect.^{16–18,21} In the present paper, we propose a multiscale simulation, named synchronized molecular dynamics simulation (SMD), for the coupled heat and momentum transfer in polymer lubrication by extending the

multiscale simulation for momentum transport. By using this method, we investigate the rheological properties and conformation of polymer chains in thermohydrodynamic lubrication of a polymeric liquid composed of short chains in a gap between parallel plates, in which the width of the gap is so large that the macroscopic quantities, e.g., velocity, stress and temperature, become spatially heterogeneous.

In the following, we first describe the problem considered in the present paper. The simulation method is explained after the presentation of the problem. The SMD simulation of polymer lubrication is performed, and the results are discussed; these results are mainly the rheological properties and the coupling of the conformations of the polymer chains with heat generation under shear flows. Finally, a short summary and a perspective on the future of SMD are given.

We consider a polymeric liquid contained in a gap with a width H between parallel plates with a constant temperature T_0 . The polymeric liquid is composed of short Kremer-Grest chains²⁵ of ten beads, in which all of the bead particles interact with a truncated Lennard-Jones potential defined by $U_{LJ}(r) = 4\epsilon \left[\left(\frac{\sigma}{r}\right)^{12} - \left(\frac{\sigma}{r}\right)^6 \right] + \epsilon$, for $r \leq 2^{1/6}\sigma$, and 0, for $r > 2^{1/6}\sigma$, and consecutive beads on each chain are connected by an anharmonic spring potential, $U_F(r) = -\frac{1}{2}k_e R_0^2 \ln \left[1 - \left(\frac{r}{R_0}\right)^2 \right]$, with $k_e = 30\epsilon/\sigma^2$ and $R_0 = 1.5\sigma$. The polymeric liquid is in a quiescent state with a uniform density ρ_0 and a uniform temperature T_0 before a time $t = 0$. Hereafter, the y -axis is perpendicular to the parallel plates and the boundaries between the upper and lower plates and the polymeric liquid are located at $y = H$ and 0, respectively. The

*Electronic mail: yasuda@sim.u-hyogo.ac.jp

†Electronic mail: ryoichi@cheme.kyoto-u.ac.jp

upper plate starts to move in the x -direction with a constant shear stress σ_0 at a time $t=0$ while the lower plate is at rest.

The macroscopic behavior of the polymeric liquid is described by the fluid-dynamic equations.

$$\rho_0 \frac{\partial v_x}{\partial t} = \frac{\partial \sigma_{xy}}{\partial y}, \quad (1a)$$

$$\rho_0 \frac{\partial e}{\partial t} = \sigma_{xy} \dot{\gamma} - \lambda \frac{\partial^2 T}{\partial y^2}, \quad (1b)$$

where v_α is the velocity, $\sigma_{\alpha\beta}$ is the stress tensor, e is the internal energy per unit mass, and $\dot{\gamma}$ is the shear rate; i.e., $\dot{\gamma} = \partial v_x / \partial y$. Hereafter, the subscripts α , β , and γ represent the index in Cartesian coordinates; i.e., $\{\alpha, \beta, \gamma\} \in \{x, y, z\}$. Here, we assume that the macroscopic quantities are uniform in the x and z directions, $\partial/\partial x = \partial/\partial z = 0$ and that the density of polymeric liquid is constant. Fourier's law for heat flux with a constant and uniform thermal conductivity λ is also considered in Eq. (1b). We also assume that the velocity and temperature of the polymeric liquid are the same as those of the plates at the boundaries, i.e., the non-slip and non-temperature-jump boundary condition.

The effect of viscous heating is estimated by the ratio of the first and second terms in Eq. (1b) to be $\sigma_0 \dot{\Gamma} H^2 / \lambda \Delta T_0$. Here, $\dot{\Gamma}$ is the gross shear rate of the system defined by the ratio of the velocity of the upper plate v_w to the width of the gap H , $\dot{\Gamma} = v_w / H$, and ΔT_0 is a characteristic temperature rise for the polymeric liquid. In the present problem, we consider a characteristic temperature necessary to substantially change the viscosity of polymeric liquid; i.e., $\Delta T_0 = |\eta_0 / (\partial \eta_0 / \partial T_0)|$, where η_0 is the characteristic viscosity of the polymeric liquid at a temperature of T_0 . Thus, the Nahme-Griffith number Na , defined to be

$$Na = \frac{\sigma_0 \dot{\Gamma} H^2}{\lambda |\partial \log(\eta_0) / \partial T_0|^{-1}} \quad (2)$$

represents the effect of viscous heating on the changes in the rheological properties.^{3,26} Usually, in lubrication systems and in high-speed processing operations with polymeric liquids, the Nahme-Griffith number is not negligibly small because of the large viscosity and the small thermal conductivity of the polymeric liquid.²⁶ For example, when a lubrication oil in a gap with a width of $1 \mu\text{m}$ is subjected to shear deformation with a strain rate of $1 \times 10^6 \text{ s}^{-1}$, the Nahme-Griffith number is estimated to be $Na \gtrsim 0.1$. Thus, the rheological properties of the lubricant in such micro devices must be not only significantly affected by the large velocity gradient but also by the temperature rise caused by local viscous heating. To predict the rheological properties of the polymeric liquid in these systems, one must consider the temperature variation of Eq. (1b) coupled with Eq. (1a).

In the present simulation, the gap between the parallel plates is divided into M mesh intervals with a uniform

width of $\Delta y = H/M$, and the local velocities are calculated at each mesh node through the typical finite volume scheme in Eq. (1a). The local shear stresses $\sigma_{xy}(y)$ are calculated from the local shear rates in the MD cells associated with each mesh interval by using the NEMD simulation with the SLLOD algorithm. The MD simulations are performed in a time interval Δt , and the time integrals of the instantaneous shear stresses \mathcal{P}_{xy} in each MD cell are used to update the local velocities at the next time step in accordance with the macroscopic momentum transport Eq. (1a),

$$v_x^n(y) = v_x^{n-1}(y) + \frac{\partial}{\partial y} \int_{(n-1)\Delta t}^{n\Delta t} \mathcal{P}_{xy}(\tau; \dot{\gamma}^{n-1}(y)) d\tau. \quad (3)$$

Here, the superscript n represents the time step number, $\mathcal{P}_{xy}(\tau; \dot{\gamma}^{n-1}(y))$ is the instantaneous shear stress in the NEMD simulation with a shear rate of $\dot{\gamma}^{n-1}(y)$, and τ is the temporal progress of the NEMD simulation. Note that the time-step size of MD simulation is different from Δt . The local viscous heating caused by shear flow, i.e., the first term of Eq. (1b), is calculated in the NEMD simulations without the use of a thermostat algorithm in each MD cell, but, at each time interval Δt , the instantaneous kinetic energies of the molecules per unit mass \mathcal{K} in each MD cell are corrected according to the heat fluxes between neighbor MD cells through $\delta\mathcal{K} = -\frac{\lambda}{\rho_0} \frac{\partial^2}{\partial y^2} \int_{(n-1)\Delta t}^{n\Delta t} \mathcal{T}(\tau) d\tau$, where \mathcal{T} is the instantaneous temperature of the MD cell. Thus, the MD simulations assigned to each fluid element are synchronized at each time interval Δt to satisfy the macroscopic heat and momentum transport equations. Note that it is difficult to rewrite Eq. (1b) as the time evolution of temperature in general because the internal energy depends on not only the macroscopic variables but also the conformations of the polymer chains. In the present SMD simulation, the temperature rise caused by local viscous heating is calculated autonomously in the MD simulation and satisfies the macroscopic energy balance of Eq. (1b).

Hereafter, we measure the length, time, temperature and density in units of σ , $\tau_0 = \sqrt{m\sigma^2/\epsilon}$, ϵ/k_B , and m/σ^3 , respectively. Here k_B is the Boltzmann constant, and m is the mass of the LJ particle. In the following simulations, the density and thermal conductivity of the polymeric liquid are fixed to be $\rho_0 = 1$ and $\lambda=150$, respectively, and the temperature of the plates and the width of the gap between the plates are fixed to be $T_0 = 0.2$ and $H = 2500$, respectively, whereas the shear stress applied to the upper plate σ_0 varies. At this number density ρ_0 and temperature T_0 , the configuration of the bead particles becomes severely jammed and results in the complicated rheological properties.^{18,27} The number of mesh intervals M and the time interval Δt are $M=64$ and $\Delta t=1$, respectively. One hundred polymer chains of ten beads, i.e., one thousand bead particles, are contained in each MD cell. Thus, the mesh width and side length of the MD cell are $\Delta y=39.0625$ and $l_{\text{MD}}=10$, respectively. The time-step size in the MD simulation $\Delta\tau$

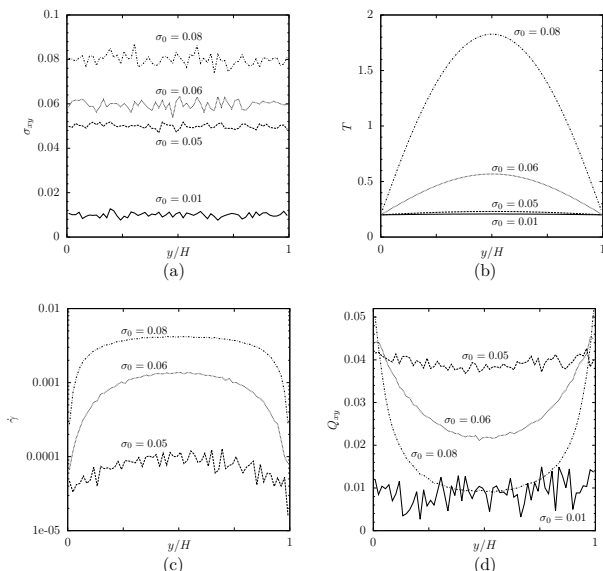


FIG. 1: The spatial variation in the shear stress $\sigma_{xy}(y)$ (a), temperature $T(y)$ (b), shear rate $\dot{\gamma}(y)$ (c), and xy component of the bond orientation tensor in Eq. (4) (d) for various values of σ_0 .

is set to be $\Delta\tau = 0.001$. Thus, MD simulations are performed for one thousand time steps in the time interval Δt , i.e., $\Delta t = 1000\Delta\tau$.

We performed multiscale simulations with various values for the shear stress applied to the plate σ_0 , i.e., $\sigma_0 = 0.002, 0.01, 0.03, 0.05, 0.055, 0.06, 0.07, 0.08$, and 0.09 and investigated the behaviors of a polymeric liquid in the steady state. In the following, we present quantities averaged for a long time in the steady state, in which the shear stress is spatially uniform and the time derivative of the local internal energy, i.e., the left-hand side of Eq. (1b), is negligible.

Figure 1 shows the spatial variations of local quantities for various values of the shear stress applied to the plate, i.e., for $\sigma_0 = 0.01, 0.05, 0.06$, and 0.08 . The shear stress σ_{xy} is found to be spatially uniform, and this fact also indicates that the condition necessary for the polymeric liquid to be in the steady state is satisfied in the present simulation. The spatial variation of the temperature T is small when the applied shear stress σ_0 is smaller than 0.05 , $\sigma_0 \leq 0.05$ whereas, for $\sigma_0 \geq 0.06$, the spatial variation in T becomes notable. The spatial variation in the shear rate $\dot{\gamma}$ also increases rapidly when the applied shear stress σ_0 is larger than 0.05 . However, the behaviors of spatial variation of temperature and shear rate are different. The spatial variation in the shear rate is only enhanced in the vicinity of the plate and is rather moderate except in the vicinity of the plate whereas the spatial variation in the temperature is a parabolic curve throughout the region. Note that, in Fig. 1(c), we omit the result for $\sigma_0 = 0.01$ because the amplitude of the shear rate is very small and occasionally exhibits negative val-

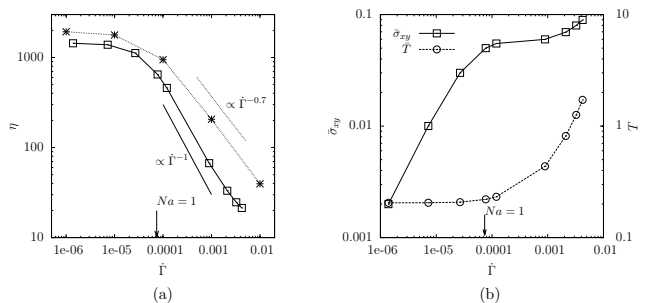


FIG. 2: The apparent viscosity η , defined to be $\eta = \sigma_0/\dot{\Gamma}$ (a) and the spatial averages of the shear stress and temperature, $\bar{\sigma}_{xy}$ and \bar{T} , (b) as a function of the gross shear rate $\dot{\Gamma}$. In figure (a), the asterisks “*” show the results of viscosity for a uniform temperature $T = 0.2$, i.e., $Na = 0$, obtained by the NEMD simulations. The downward arrows in both figures represent the shear rate at which the Nahme-Griffith number Na defined in Eq. (2) equals unity.

ues from the fluctuations; the spatial average of the shear rate for $\sigma_0 = 0.01$ is 7.2×10^{-6} . In Fig. 1(d), we show the xy component of the bond orientation tensor Q_{xy} defined to be

$$Q_{\alpha\beta} = \frac{1}{M_p} \sum_{\text{chain}} \frac{1}{N_b - 1} \sum_{j=1}^{N_b-1} \frac{b_{j\alpha} b_{j\beta}}{b_{\min} b_{\min}}, \quad (4)$$

where M_p is the number of polymer chains in each MD cell, N_b is the number of bead particles on a polymer chain, \mathbf{b}_j for $1 \leq j \leq N_b - 1$ is the bond vector between consecutive beads on the same chain, and b_{\min} is the distance at which the sum $U_{LJ}(r) + U_F(r)$ has a minimum and is calculated to be $b_{\min} \simeq 0.97$. The spatial variation in Q_{xy} is also small for small applied shear stresses, i.e., $\sigma_0 \leq 0.05$, but this spatial variation becomes notable for $\sigma_0 \geq 0.06$. In the vicinity of the plate, Q_{xy} increases monotonically with the applied shear stress σ_0 whereas, in the middle of the plates, Q_{xy} varies non-monotonically with the applied shear stress. This complicated behavior arises from the temperature variation; the conformation of the polymer chains in the vicinity of the plate is primarily involved in the shear rate because the temperature variation is small there, but, at the middle of the plates, the conformation of the polymer chains is mainly influenced by the temperature because the temperature variation is large there. The relations among the temperature, shear rate, and conformation of polymer chains is also discussed in detail later.

In the following, we investigate the rheological properties of the system. Hereafter, the spatial average of a quantity $a(y)$ is represented as \bar{a} , i.e., $\bar{a} = \frac{1}{H} \int_0^H a(y) dy$. Figure 2 shows the apparent viscosity of the system and the spatial averages of the shear stress and temperature as a function of the gross shear rate. The downward arrows in Fig. 2 indicate the reference shear rate at which the Nahme-Griffith number Na defined in Eq. (2) equals unity, where the reference temperature is calculated from

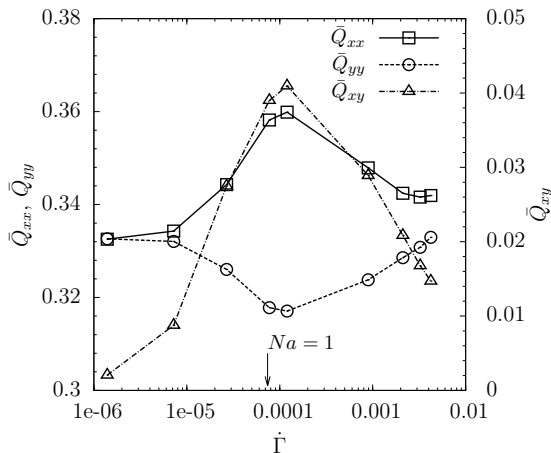


FIG. 3: The spatial average of the bond orientation tensor of the polymer chains $\bar{Q}_{\alpha\beta}$ as a function of the gross shear rate $\dot{\Gamma}$. Also see the caption in Fig. 2

the viscosities of the model polymeric liquid obtained by the NEMD at the uniform and constant temperatures $T = 0.2$ and 0.4 in Ref. 27 as $\Delta T_0 = 0.15$. In Fig 2(a), the apparent viscosity is compared to the viscosity of a polymeric liquid with a uniform and constant temperature T_0 obtained from the NEMD simulation; this case corresponds to a negligible Nahme-Griffith number, $Na = 0$. Strong shear thinning occurs when the Nahme-Griffith number exceeds unity, $Na > 1$. The slope in the power law, i.e., the index ν in the approximate relation $\eta(\dot{\Gamma}) \propto \dot{\Gamma}^{-\nu}$, is almost unity (but never exceeds unity), $\nu \simeq 1$, for $\dot{\Gamma} = 1 \times 10^{-4} \sim 1 \times 10^{-3}$. A discrepancy between the apparent viscosity and that for $Na = 0$ is thought to be caused by the fact that the temperature slightly increases in the present simulation even at the smallest gross shear rate (the average temperature \bar{T} increases 2.5 percent of the wall temperature T_0) and the temporal-spatial fluctuations of temperature and shear rate are also induced in the present simulation whereas the temperature and shear rate are kept constant and uniform in the NEMD simulation. Figure 2(b) shows the spatial averages of the local shear stress and temperature as a function of the gross shear rate. We note that the spatial average of the shear stress $\bar{\sigma}_{xy}$ coincides with the applied shear stress σ_0 on the plate because the local shear stress is almost spatially uniform in the steady state, as shown in Fig. 1(b). The average shear stress $\bar{\sigma}_{xy}$ is seen to increase monotonically with the gross shear rate. The plateau region of the curve corresponds to the strongly shear-thinning regime with the index $\nu \simeq 1$ in Fig. 1 (a). The average temperature increases rapidly with the gross shear rate when the Nahme-Griffith number exceeds unity. The rate of increase for the average temperature is lower than that for the average shear stress at small gross shear rates, $\dot{\Gamma} \lesssim 1 \times 10^{-4}$, but reverses at large gross shear rates, $\dot{\Gamma} \gtrsim 1 \times 10^{-4}$.

Figure 3 shows the conformation changes of the poly-

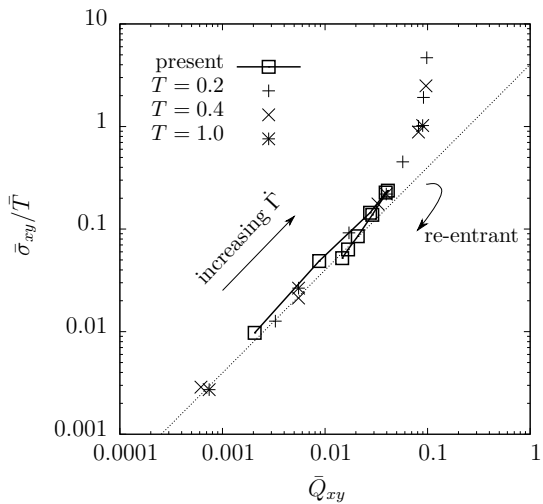


FIG. 4: The stress-optical relation $\bar{\sigma}_{xy}/\bar{T}$ vs. \bar{Q}_{xy} . The squares \square show the present results, and the symbols $+$, \times , and $*$ show the results obtained in Ref. 27 at uniform temperatures.

mer chains as a function of the gross shear rate. A non-monotonic dependence of the conformation of polymer chains on the gross shear rate is observed. A transition occurs at the entrance to the strong shear-thinning regime with $\nu \simeq 1$ in Fig. 2(a), i.e., $\dot{\Gamma} \simeq 1 \times 10^{-4}$. The polymer chains are stretched in the x direction, and the xy component of the bond orientation tensor increases as $\dot{\Gamma}$ for small gross shear rates, $\dot{\Gamma} \lesssim 1 \times 10^{-4}$. However, for large gross shear rates, $\dot{\Gamma} \gtrsim 1 \times 10^{-4}$, the alignment of the polymer chains is disturbed, and the conformation of polymer chains becomes more isotropic as the gross shear rate increases. This transitional behavior is caused by the temperature variation; the temperature increases sufficiently for the large gross shear rates, so that the coherent structure is disturbed by the thermal motion of the bead particles.

Figure 4 shows the stress-optical relation for the present problem.²⁸⁻³⁰ For the present model polymeric liquid, the NEMD simulations for the isothermal shear flows, i.e., $Na=0$, clarified that a universal curve in the stress-optical relation holds in both the linear ($\bar{Q}_{xy} \lesssim 0.05$) and nonlinear ($\bar{Q}_{xy} \gtrsim 0.05$) regimes.²⁷ In the figure, the present results are compared with those for the case $Na = 0$. The leftmost square symbol for the present study represents the result for the smallest gross shear rate, i.e., $\dot{\Gamma} \simeq 1 \times 10^{-6}$. It is seen that $\bar{\sigma}_{xy}/\bar{T}$ increases with \bar{Q}_{xy} while the gross shear rate increases up to $\dot{\Gamma} \lesssim 1 \times 10^{-4}$ because the shear stress increases more rapidly with the gross shear rate than the temperature (see Fig. 2(b)) and \bar{Q}_{xy} also increases with the gross shear rate in this regime (see Fig. 3). However, for large gross shear rates, i.e., $\dot{\Gamma} \gtrsim 1 \times 10^{-4}$, the temperature increases more rapidly than the shear stress, and the xy component of the bond orientation tensor decreases with the gross shear rate. Interestingly, the linear stress-

optical relation is recovered for shear stresses larger than that for the transitional behavior of the conformational tensor, although the temperature, shear stress, and conformation of the polymer chains exhibit very complicated nonlinear behavior. This reentrant transition of the linear stress-optical relation for large shear stresses can be never reproduced in the NEMD simulations with a thermostat because both the shear stress $\bar{\sigma}_{xy}$ and the xy component of the bond orientation tensor \bar{Q}_{xy} monotonically increase with the shear rate at a constant temperature \bar{T} but \bar{Q}_{xy} saturates to a limiting value, $\bar{Q}_{xy} \sim 0.1$, so the nonlinear stress-optical relation forms as shown in Fig. 4 for the case $Na = 0$.

In summary, we proposed the synchronized molecular dynamics simulation via macroscopic heat and momentum transfer, and applied this method to the analysis of the lubrication of a polymeric liquid coupled with viscous heating. The rheological properties and the conformations of the polymer chains are investigated with a non-dimensional parameter, i.e., the Nahme-Griffith number. The SMD simulation demonstrates that strong shear thinning, which is almost inversely proportional to the shear rate, and the transitional behavior for the conformation of the polymer chains occur with a rapid temperature rise when the Nahme-Griffith number exceeds unity. The results clarify that the linear stress-optical

relation holds despite the complicated behaviors of the temperature, the shear rate, and the conformation of the polymer chains.

The SMD simulation has two distinctive advantages over the full MD simulations; First, the SMD simulation can reduce the computational effort (i.e., the number of molecules) compared to that of the full MD simulation by a factor of $(l_{\text{MD}}/\Delta x)^d$ where d is the dimension number of the macroscopic transport equation. In the present simulation, the factor is approximately a quarter because d is one. However, the extension to the two- and three-dimensional case is also possible by incorporating the algorithms developed in Refs. 15 and 12–14, for example. Secondly, almost perfect parallelization efficiency is achieved in a parallel computation with as many CPUs as MD cells by assigning the CPUs to each MD cell. This efficiency is reached because each MD simulation is performed independently in the time interval Δt . The advantage in parallel computation holds not only for the short-range interaction molecular models but also for any complicated molecular models for which the parallelization of MD simulations is difficult. These advantages make it possible for us to analyze the complicated flow behaviors of complex liquids at the macroscopic scales found in actual engineering and biological systems on the basis of the appropriate molecular model.

-
- ¹ M. P. Allen and D. J. Tildesley, *Computer Simulation of Liquids*, (Oxford University Press, New York, 1989).
- ² D. J. Evans and G. Morris, *Statistical mechanics of nonequilibrium liquids*, (Cambridge university press, New York, 2008).
- ³ R. B. Bird, R. C. Armstrong, and O. Hassager, *Dynamics of polymeric liquids* Vol. 1 (John Wiley and Sons, New York, 1987).
- ⁴ M. Laso and H. C. Öttinger, *J. Non-Newtonian Fluid Mech.* **47**, 1 (1993).
- ⁵ K. Feigl, M. Laso, and H. C. Öttinger, *Macromolecules* **28**, 3261 (1995).
- ⁶ M. A. Hulsen, E. A. J. F. Peters and B. H. A. A. van den Brule: *J. Non-Newton. Fluid Mech.* **98** (2001) 201.
- ⁷ W. E and B. Engquist, *Comm. Math. Sci.* **1**, 87 (2003).
- ⁸ I. G. Kevrekidis, C. W. Gear, J. M. Hyman, P. G. Kevrekidis, O. Runborg, and C. Theodoropoulos, *Comm. Math. Sci.* **1**, 715 (2003).
- ⁹ W. Ren and W. E, *J. Compt. Phys.* **204**, 1 (2005).
- ¹⁰ S. De, J. Fish, M. S. Shephard, P. Koblinski, and S. K. Kumar, *Phys. Rev. E* **74**, 030801(R) (2006).
- ¹¹ D. A. Kessler, E. S. Oran, and C. R. Kaplan, *J. Fluid Mech.* **661**, 262 (2010).
- ¹² T. Murashima and T. Taniguchi, *J. Polym. Sci. B* **48**, 886 (2010).
- ¹³ T. Murashima and T. Taniguchi, *Europhys. Lett.* **96**, 18002 (2011).
- ¹⁴ T. Murashima and T. Taniguchi, *J. Phys. Soc. Jpn.* **81**, SA013 (2012).
- ¹⁵ S. Yasuda and R. Yamamoto, *Phys. Fluids* **20**, 113101 (2008).
- ¹⁶ S. Yasuda and R. Yamamoto, *Europhys. Lett.* **86**, 18002 (2009).
- ¹⁷ S. Yasuda and R. Yamamoto, *Phys. Rev. E* **81**, 036308 (2010).
- ¹⁸ S. Yasuda and R. Yamamoto, *Phys. Rev. E* **84**, 031501 (2011).
- ¹⁹ M. Müller and K. C. Daoulas, *Phys. Rev. Lett.* **107**, 227801 (2011).
- ²⁰ M. Salloum, K. Sargsyan, R. Jones, B. Debusschere, H. N. Najm, and H. Adalsteinsson, *Multiscale Model. Simul.* **10**, 550 (2012).
- ²¹ T. Murashima, S. Yasuda, T. Taniguchi, and R. Yamamoto, *J. Phys. Soc. Jpn.* **82**, 012001 (2013).
- ²² E. Brini, E. A. Algaer, P. Ganguly, C. Li, F. Rodriguez-Ropero and N. F. A. van der Vegt, *Soft Matter* **9**, 2108 (2013).
- ²³ S. De, *Phys. Rev. E* **88**, 052311 (2013).
- ²⁴ M. K. Borg, D. A. Lockerby, J. M. Reese, *J. Compt. Phys.* **233**, 400 (2013).
- ²⁵ K. Kremer and G. S. Grest, *J. Chem. Phys.* **92**, 5057 (1990).
- ²⁶ C. J. Pipe, T. S. Majmudar, and G. H. McKinley, *Rheol. Acta* **47**, 621 (2008).
- ²⁷ R. Yamamoto and A. Onuki, *J. Chem. Phys.* **117**, 2359 (2002).
- ²⁸ H. Janeschitz-Kriegl, *Polymer Melt Rheology and Flow Birefringence* (Springer, Berlin, 1983).
- ²⁹ M. Doi and S. F. Edwards, *The theory of polymer dynamics* (Clarendon, Oxford, 1986).
- ³⁰ G. Strobl, *The Physics of polymers* (Springer, Heidelberg, 2007).